Proceedings of ASME Turbo Expo 2011
GT2011
June 6-10, 2011, Vancouver, British Columbia, Canada

GT2011-46223

IMPELLER – VANED DIFFUSER INTERACTION IN A CENTRIFUGAL COMPRESSOR AT THE BEST EFFICIENCY POINT

P. Gaetani, G. Persico, A. Mora, V. Dossena, C. Osnaghi
Laboratorio di Fluidodinamica delle Macchine, Dipartimento di Energia, Politecnico di Milano
Via Lambruschini, 4 – 20158 - Milano, Italy
www.lfm.polimi.it
paolo.gaetani@polimi.it

ABSTRACT

Centrifugal compressors find a huge number of applications in industry and in aero-engines; the detailed comprehension of the complex fluid-dynamic mechanisms occurring in these machines is crucial to improve their efficiency and their operating range. The paper presents a study on the impeller – vaned diffuser interaction in a high-performance compressor stage, in the frame of a wide experimental campaign devoted to the comprehension of unsteady flows in centrifugal compressor stages. The paper focuses on the best efficiency operating point. Data were collected in the impeller - vaned diffuser gap by applying a fast response probe. The impeller runs at 12500 RPM and the peripheral Mach number is 0.77.

At first, data are reduced to highlight the main flow structures released by the impeller. CFD simulations – first verified against experimental data – were also performed to get detailed information of the flow field inside the impeller. The core of the paper is the discussion of the impeller - diffuser interaction. Results evidence the effect of the diffuser on the impeller in terms of static pressure and flow velocity. Moreover, the interaction process makes the average flow rate discharged by an impeller channel and the power exchange to be unsteady.

INTRODUCTION

Centrifugal compressors are commonly used in many industrial applications, such as the oil and gas and process plants, and some aero-engines. Reviews on application and design of centrifugal compressors can be found in [1-3].

Besides providing acceptable efficiency levels, the success of centrifugal compressors against axial machines are to be find in the reduced axial dimensions, the intrinsic higher reliability and their wider operational range.

The assessment of the stage performance is of fundamental importance for the machine designers, and much effort was spent and will be spent, on increasing the accuracy and design tool predictability (see, among the others [4, 5]). Experimental activities are a key-phase in this process. In order to improve the efficiency and enlarge the operating range, an in-depth comprehension of the flow field of both the impeller and the diffuser and of their interaction is to be achieved. Many studies were performed in the last decades on the topic and some of them on high speed compressors. Most of the experimental works were based on optical techniques [6, 7], while, to the knowledge of the authors, in only one case Fast Response Probes were used [8].

Many studies on the impeller flow ([9, 10] among the many) evidenced the 3D character of the flow discharged by the impeller, often reduced to the jet/wake scheme. The dissipative region connected to the action of the secondary flow – whose magnitude and extension depends on the operational point and on the geometry - accumulates mainly on the tip-suction side corner of the impeller channel at the outlet section.

When the impeller-vaned diffuser interaction is of concern, the number of studies available in the open literature reduces, as the complexity of the measurement techniques and of the test rigs increases. Some studies [11] concentrate on the propagation of the diffuser perturbation within the impeller passage. Other studies [12, 13] focus on the influence of non uniform flows on diffuser performances.

In the authors' opinion there are still open issues in the comprehension of the interaction mechanism between the impeller flow (jet/wake, potential and secondary flow patterns) and the vaned diffuser potential field. Furthermore, the production of detailed experimental data bases are of great importance to assess and improve CFD tools, both 1D and 3D, commonly used in the compressor design.

In this context, a wide research activity was started up at the Laboratorio di Fluidodinamica delle Macchine (LFM) of the Politecnico di Milano. The measurement campaign was performed at three different flow rates. In this paper only results at the best efficiency point are reported and discussed, focusing on the interaction mechanism. Measurements were performed by means of a Fast Response Aerodynamic Pressure Probe (FRAPP), widely applied in the last ten years at LFM.

Coupled to the experimental activities, CFD calculations of the impeller flow were performed in order to support and to enhance the flow phenomena comprehension.

EXPERIMENTAL SETUP

Test rig:

The experimental work was performed at the Laboratorio di Fluidodinamica delle Macchine of the Politecnico di Milano, on a closed loop test rig for compressors and turbines, whose general layout is depicted in Fig. 1A.

The test campaign was carried out in the centrifugal section using air as working fluid and imposing the ambient pressure at the stage inlet. The tested impeller is a centrifugal transonic un-shrouded rotor with radial discharge section (Fig. 1B). The main test rig characteristics are reported in Tab. 1. The impeller and the diffuser parameters are reported in Tab. 2; the diffuser height being greater than the impeller blade height, the configuration has a smoke-shelf at the tip side (Fig. 2). The smoke-shelf solution was considered a promising technique to enhance the flow mixing prior its entrance in the diffuser. Such geometry was studied in a previous research program and was kept identical for the present one because it has a weak effect on the interaction mechanism, as discussed in the following sections.

The test rig is instrumented to allow flange-to-flange measurements, as well as detailed analyses of the flow inside the impeller, at the impeller discharge and inside the diffuser. In order to allow impeller – vaned diffuser interaction analyses, the diffuser can be rotated by a stepping motor. The diffuser discharges the flow in a volute characterised by a rectangular section that acts as a plenum. Measurements were taken by means of a Fast Response Aerodynamic Pressure Probe (FRAPP) at four radial positions (R1: d/D_2=1.025, R2: d/D_2=1.045, R3: d/D_2=1.065, R4: d/D_2=1.085), for 15 tangential positions on the diffuser pitch and for 12 points on the blade height at the best efficiency point.

Max. Power	800 kW
Max. rotational speed	18000
Max. impeller diameter	560 mm
Max. compression ratio	2.5

Table 1: main test rig parameters

IMPELLER		VANED DIFFUSER	
Tip inlet diameter	262 mm	Inlet diameter	440 mm
Outlet diameter	400 mm	Outlet diameter	765 mm
Blade height	17.4 mm	Vane height	22 mm
Outlet blade angle	- 24 deg	Inlet blade angle	63 deg.
N° of blades	16	N° of vanes	25
OPERATING CONDITIONS			
Peripheral Mach number: $Mu = U_2 / a_0 = 0.775$		Rotational speed [RPM]: 12500	
Inlet Flow coefficient: $Q / U_2 / D_2^2 = 0.063$		Total pressure ratio: 1.605	

Table 2: geometrical and operational data

Due to the probe head design and the need of rotating the diffuser, the minimum distance of the pressure tap from the hub is 5.6 mm over a blade height of 17.4 mm. Regarding the test-rig instrumentation, the compressor head was measured by two transducers connected to pressure taps at the inlet and outlet of the machine. The flow rate was measured by a Venturi nozzle manufactured according to the EN ISO 5167-3 standard. The rotational speed was taken by a pick-up located on the compressor shaft. The same device was also used as key-phasor for the phase-resolved measurements. Temperatures at the compressor inlet and outlet were measured by shielded K and T type thermocouples. Finally time-mean temperature

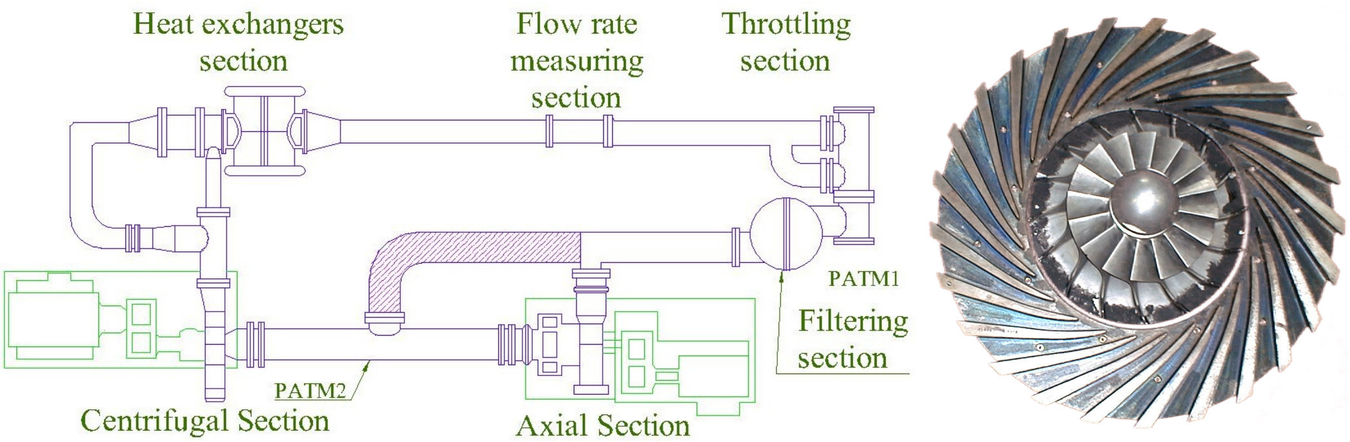

Figure 1. A) TEST RIG GENERAL LAYOUT. PATM2 = ATMOSPHERIC SINK B) IMPELLER AND DIFFUSER GEOMETRY

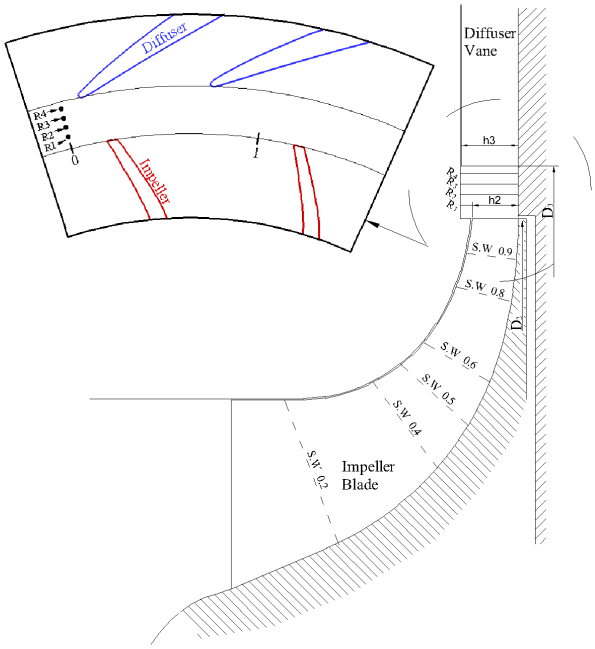

Figure 2. MERIDIONAL CHANNEL VIEW. DETAIL OF MUTUAL IMPELLER – DIFFUSER POSITION AT t/T = 0.

measurements in the impeller – diffuser gap were taken by a total temperature Kiel probe.

FRAPP:

The probe was installed at four radial positions at the exit section of the impeller in order to obtain a highly detailed flow field reconstruction.

To cope with miniaturisation requirements, the probe is developed around a single - sensor and it allows the measurements of a 2D flow field in a plane normal to the probe stem. In the present case the probe stem and the compressor shaft were parallel. Being equipped by a single transducer, the probe is applied as a virtual three-sensor probe. Phase-resolved data-reduction techniques are then required to get the flow field in terms of static and total pressure (and hence Mach number) and flow angle. Under some approximations also the turbulent kinetic energy and the flow field in the relative frame can be evaluated. Details of the techniques are reported in [14, 15]. Some applications of the same probe are reported in [16, 17].

The frequency range of the probe reaches 80 kHz after the application of a proper transfer function defined by dynamic calibration in a shock tube. The probe was calibrated for Mach numbers ranging from 0.15 to 0.75. The averaged expanded uncertainty of the pressure measurements was ±0.5% of the kinetic head, and that of the flow angle was ±0.2° over the calibration range (±22.5° from the central position).

To compensate the temperature effect on the sensor, static calibration was performed by changing the temperature in the range 0 -100 °C.

Raw pressure data were phase-locked to the rotor wheel and then phase-averaged to obtain 40 intervals on a single rotor-blade passing period. The resulting physical sample rate was ~133 kHz and matches the Nyquist criterion. As a final step, the flow properties were derived by the combination of the different phase-averaged pressures.

The unsteady flow quantities, originally measured in the absolute frame, were further converted into relative quantities making use of the measured time-averaged total temperature.

Results are first displayed as time-averaged flow field in the rotating frame. When the impeller–vaned diffuser interaction is discussed, results are displayed as snapshots of the instantaneous flow field at different impeller – vaned diffuser positions.

Figure 2 shows the position between the impeller blades and the diffuser vanes at the phase zero (or initial time): such position is arbitrary and corresponds to the negative edge of the pickup signal.

CFD setup

The calculations reported in this paper were performed employing the commercial code ANSYS-CFX 12.0. The numerical method is based on a finite-volume node-centred approach with second-order upwind discretization of convective fluxes and implicit time integration. The original k-ω turbulence model is used, corrected far from solid walls, introducing a suitable blend of k-ω and k-ε models. The convergence in the iterative solution of the resulting non-linear system is enhanced by using an algebraic multi-grid technique.

The simulations performed for this research were intended to support the comprehension on the experimental flow field just downstream of the impeller. Therefore steady-state simulations were performed for the impeller only, solving for the relative velocity and activating the apparent forces.

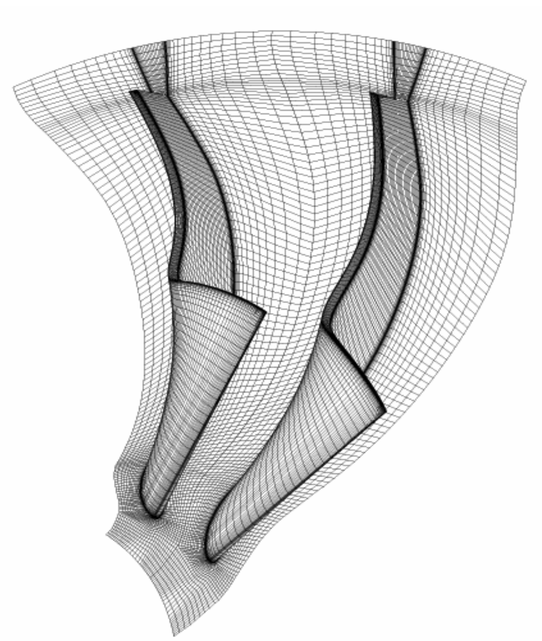

Figure 3. COMPUTATIONAL GRID

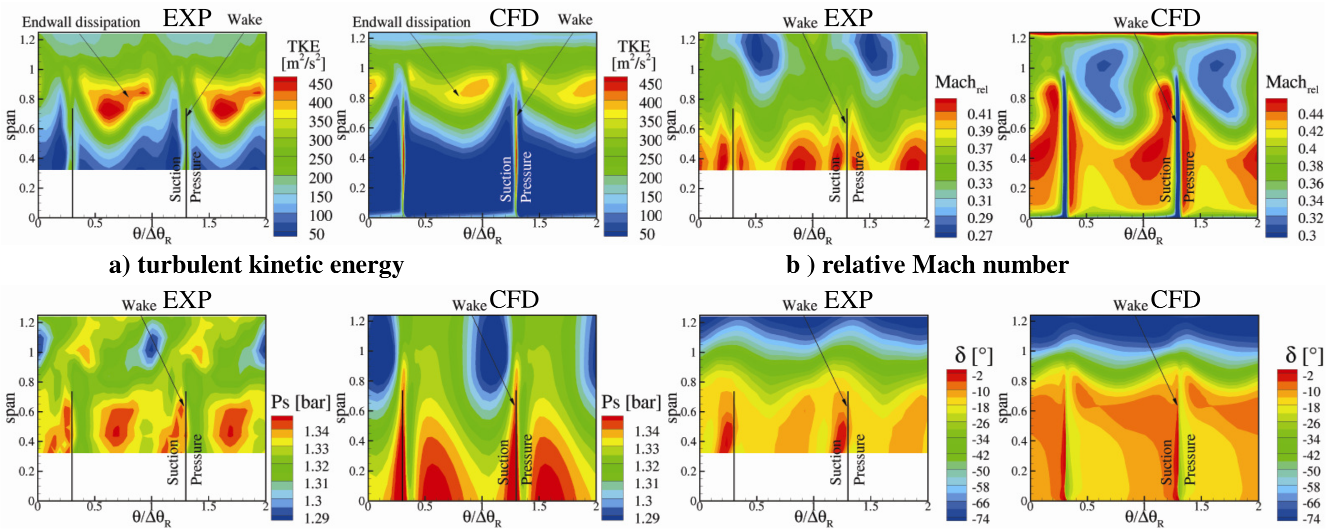

a) turbulent kinetic energy b) relative Mach number

(c) static pressure (d) deviation (slip) flow angle

Figure 4. TIME-MEAN FLOW FIELD IN THE ROTATING FRAME AT R1 – RELATIVE QUANTITIES

The computational grid is composed of hexahedral elements and was built using ANSYS/Turbogrid, following a structured multi-block strategy. An image of the grid is depicted in Figure 3, where both the hub-to-shroud and the blade-to-blade discretization can be appreciated. 92 elements are placed in spanwise direction (32 of them are in the tip clearance) and 48 elements in pitchwise direction; the resulting mesh contained about 700 kcells. Points are properly clustered in the proximity of solid walls, resulting in a y^+ close to unity on all surfaces, to satisfy the turbulence model requirements.

Uniform total pressure, total temperature and axial flow direction were imposed at the inflow. A turbulence intensity of 5% and a ratio of "turbulent" to molecular viscosity of 0.1 were also prescribed at the inlet. At the impeller outflow, placed at d/D2=1.085 (R4), static pressure is assigned. Some iteration was required to match the experimental data in terms of mass flow rate.

RESULTS

To provide an overview of the flow pattern at the impeller exit, the mean flow field in the rotating frame is first presented. For this purpose results at traverse R1 are reported in terms of relative quantities. In the second section the impeller – vaned diffuser interaction is presented and discussed.

Time-mean flow field in the rotating frame

In this section the flow field inside and downstream of the impeller is presented and discussed on the basis of experimental and numerical results. The experimental flow field, measured at the impeller exit (namely plane R1) in the stationary frame, is converted into its rotating counterpart and time-averaged in order to eliminate the effect of the vaned diffuser. Thus experimental data can be directly compared with the results of steady-state simulations.

Figure 4 reports the experimental and numerical flow field at the impeller exit, in terms of turbulent kinetic energy, relative Mach number, static pressure and deviation angle. In all frames the blade wake was traced making use of the TKE maps and on the basis of geometrical considerations.

The most explicit quantity is the TKE, derived from unsteady pressure measurements using the methodology proposed in [15]. The turbulence field marks the presence, in both the experimental and computed flow field, of two main dissipative structures discharged by the impeller: the blade wake and a loss region related to the secondary flows and tip leakage activity inside the impeller passage. To ease the CFD – EXP comparison the experimental maps in figures 4 and 8 were tangentially shifted. The spanwise and tangential position of the second loss core depends on the operating point and on the geometry: in the present case, the position is roughly at mid-pitch and not in the tip-suction side corner, as found in [10].

The generation and the evolution of such a dissipative region are now discussed on the basis of computed flow field inside the impeller. In Figg. 5 and 6 the evolution of the flow field along the impeller channel can be appreciated, in terms of turbulent kinetic energy and streamwise vorticity ($\omega_{s,rel}$, based on the relative velocity) plotted in various planes at different streamwise positions. The maps show how the tip leakage flow is the dominant three-dimensional structure inside the rotor channel. In the front part (SW 0.2 - 0.5) a wide region of high TKE and $\omega_{s,rel}$ is generated close to the suction side of the blades. This region then migrates towards the shroud endwall, finally merging with the high dissipative tip leakage flow and thus strengthening this latter structure. In the rear part of the channel (SW 0.8 - 1) this low momentum region is progressively moved towards the centre of the duct, due to the retarding effect operated by the fixed shroud; this explains why in the experiments the tip leakage flow is released by the

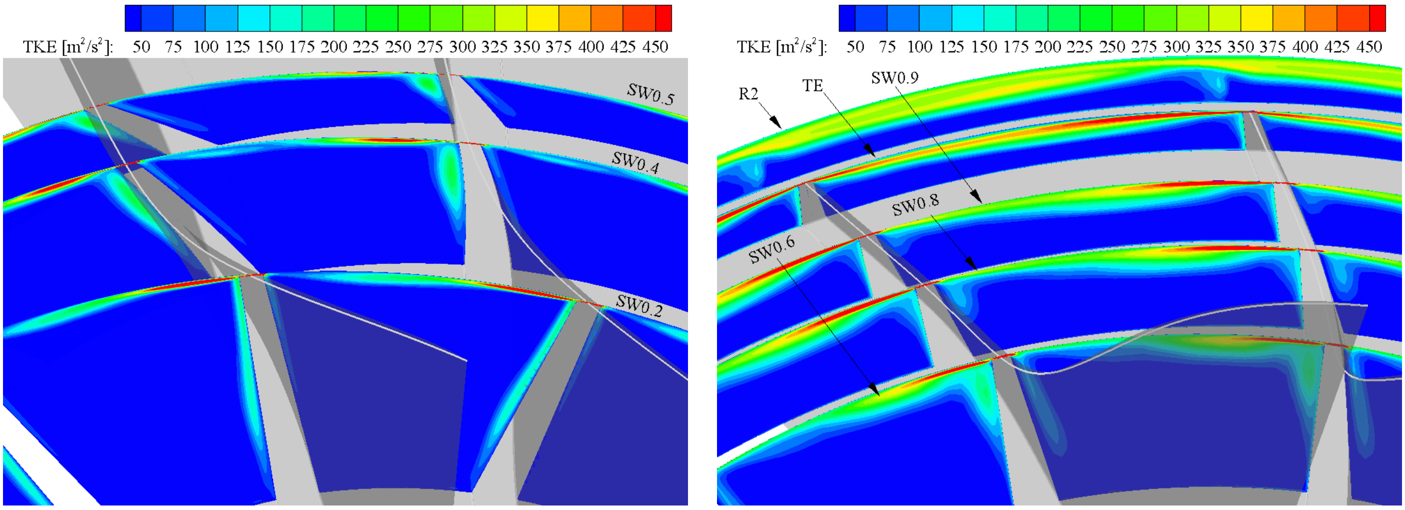

Figure 5. COMPUTED TKE DISTRIBUTION ON DIFFERENT TRAVERSES ALONG THE IMPELLER CHANNEL

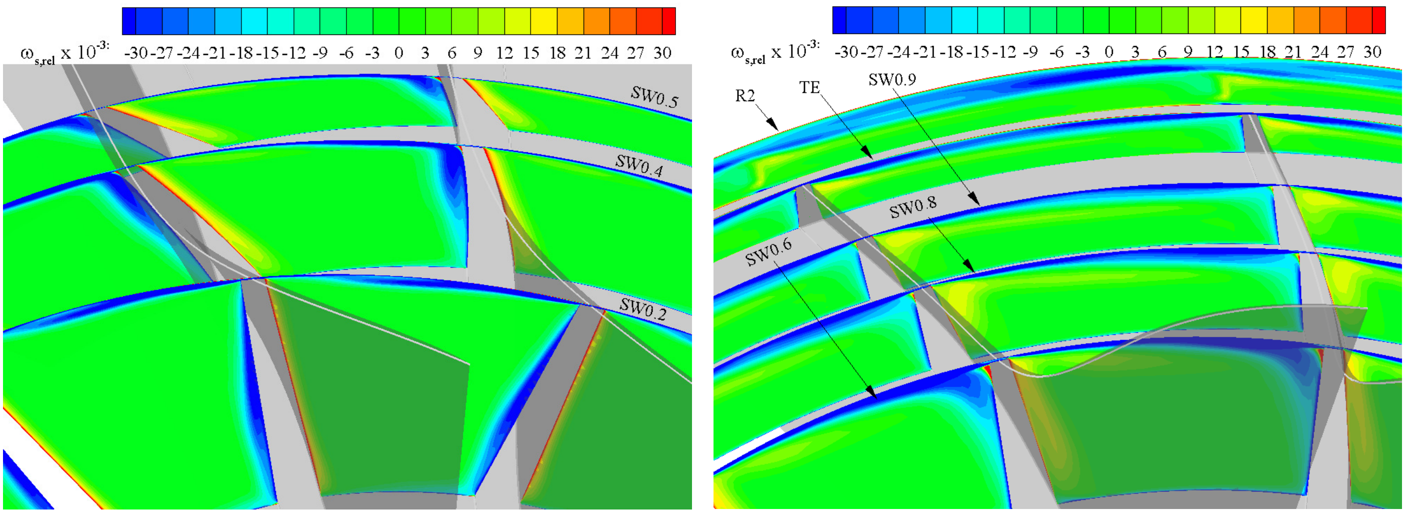

Figure 6. COMPUTED RELATIVE STREAMWISE VORTICITY DISTRIBUTION ON DIFFERENT TRAVERSES ALONG THE IMPELLER CHANNEL

impeller relatively far from the blade sides, and not concentrated on the suction side as it would have been expected by applying simplified jet/wake models. The negative vorticity region greatly enhances downstream of the trailing edge, due to the separation induced by smoke-shelf geometry (captured by the numerical model, as visible in the slip angle map).

The relative Mach number distribution reported in Fig. 4b, as also found in other applications [10], once again eludes the classical jet/wake flow scheme, either one-zone or two-zone models. The midspan-hub region is indeed characterised by wide free-stream where high velocity is found close to the suction side of the blades, interrupted by the velocity defects in the blade wake. Such feature, correctly captured by the simulation, seems to be the combination of the potential field and of the flow blockage induced by the tip leakage close to the shroud; the potential field makes the flow to be faster on the suction side than on the pressure one, while the flow blockage forces the flow to pass in adjacent regions. The tip and smoke-shelf regions have very low relative velocity due to the high dissipation induced by the leakage flow and by the sudden channel height increase.

The static pressure maps (Fig. 4c) evidence two peaks in the midspan hub region, none of them located on the blade pressure side. As for the Mach number, the dissipation dramatically reduces the pressure in the tip smoke-shelf regions and makes the pattern very complex. The numerical pressure distribution, in this case, appears to be less accurate mostly because of the small amplitude of the measured pressure variations. However, the double-oscillation observed in the experiments is also reproduced in the computed flow field. An analysis of the numerical blade-to-blade pressure distribution, reported in Fig. 7 for the midspan surface, shows that the local

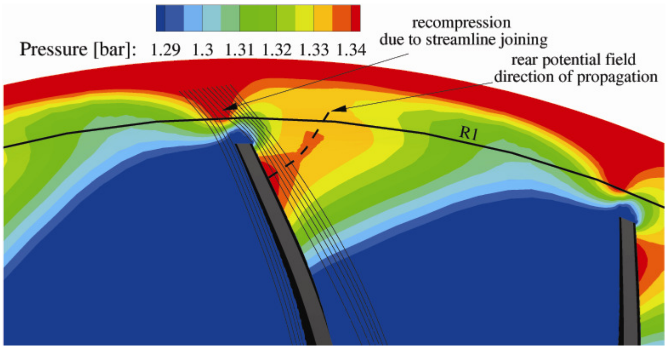

Figure 7. COMPUTED PRESSURE FIELD AT MIDSPAN

recompression on the left side of the wake is caused by the collision of the streamlines coming from the two sides of the blade just downstream of the squared trailing edge. The recompression in the centre of the channel is, instead, caused by the rear blade potential field, that propagates in direction roughly normal to the blade profile – hence very different with respect to the wake trace. The pitchwise position of the recompression zone observed in the experiments depends, therefore, on the streamwise position of traverse R1.

The deviation angle (also called slip angle, and reported in Fig. 4d) evidences that the region of the blade wake has a reduced slip, due to its high tangential component, while the tip leakage region at mid-pitch and the smoke-shelf region have very high slip. Once again the numerical model succeeds in predicting both the qualitative and quantitative feature of the flow field. It has to be noticed that $\delta < -66$ degrees indicates a radial inward velocity that means re-circulating flow. It is interesting to note that the deviation angle distribution does not show coherent vortical structures (by the application of the Rankine vortex model, which was successfully applied in other

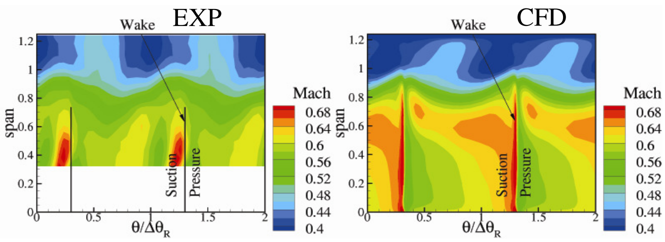

(a) absolute Mach number

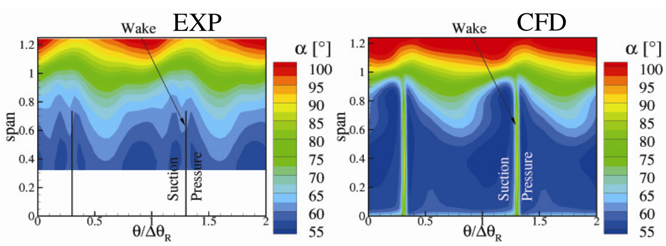

(b) absolute flow angle

Figure 8. TIME-MEAN FLOW FIELD IN THE ROTATING FRAME – ABSOLUTE QUANTITIES AT TRAVERSE R1

data analyses [10, 16]). This fact is a further confirmation of the weak role played by the secondary flows in the present impeller, with respect to the wake and the tip aerodynamics.

In the presence of a vaned diffuser, the flow structures discharged by the impeller are going to interact significantly with the front part of the subsequent vanes. As thoroughly demostrated in [11], this interaction is going to influence significantly the efficiency of the whole compressor, and thus a characterization of the absolute flow entering the diffuser is of clear interest in this study.

In Fig. 8 the time-mean absolute Mach number and flow angle in the rotating frame are reported at the entrance of the diffuser (traverse R1). Both the Mach number and flow angle maps show significant spanwise (axial) gradients, especially in the boundary between the isentropic core and the wide dissipative region in the tip / smoke-shelf region at about 90% span. The Mach number distribution also shows strong pitchwise gradients that will act as unsteady aerodynamic forces on the diffuser. Conversely, as the flow angle (especially in the experiments) has relatively small periodic oscillations, the incidence effect induced by impeller wakes is likely to play a minor role on the diffuser efficiency.

As a final remark, being the smoke-shelf effectcs confined in the tip region, such unusual geometry will not cause a loss of generality in the results here presented.

Impeller – vaned diffuser interaction

To gain insight into the impeller - vaned diffuser interaction, the streamwise (radial) evolution of the flow, in terms of absolute quantities, is now reported and discussed. Snapshots at different phases in the blade passing period are presented, taking into account the correct impeller/vane position with the reference configuration at instant t/T=0 given in Fig. 2. Before starting with the radial snapshots some spanwise profile and phase resolved flow field are discussed.

As shown in Figg. 8 and 9 the pitchwise averaged flow angle approaching the diffuser profiles is very different from hub to tip, notwithstanding the mixing that takes place in the vaneless diffuser. This leads to relevant incidence effects on the aerodynamic of the vanes in the endwall region. As the vane geometrical inlet angle (defined as the mean line angle at the leading edge) is 63 deg., the incidence angle is about –9 deg. at the hub while at the tip / smoke-shelf region it strongly rises.

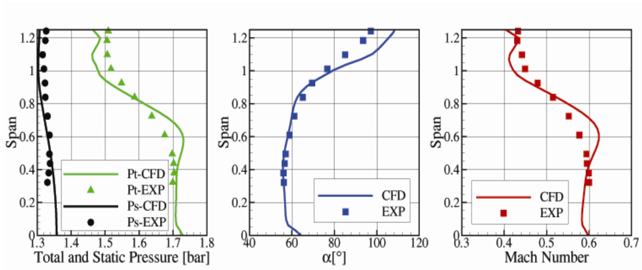

Figure 9. PITCHWISE AVERAGED PROFILES AT THE IMPELLER EXIT – DIFFUSER INLET (TRAVERSE R2)

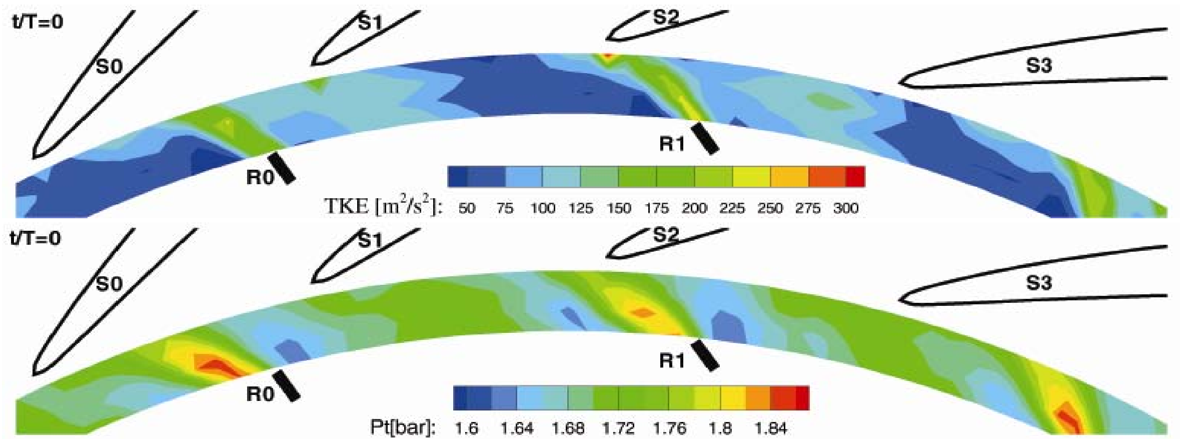

Figure 10. TKE (TOP) AND PT (BOTTOM) SNAPSHOTS AT t/T=0, h/h_2=38%

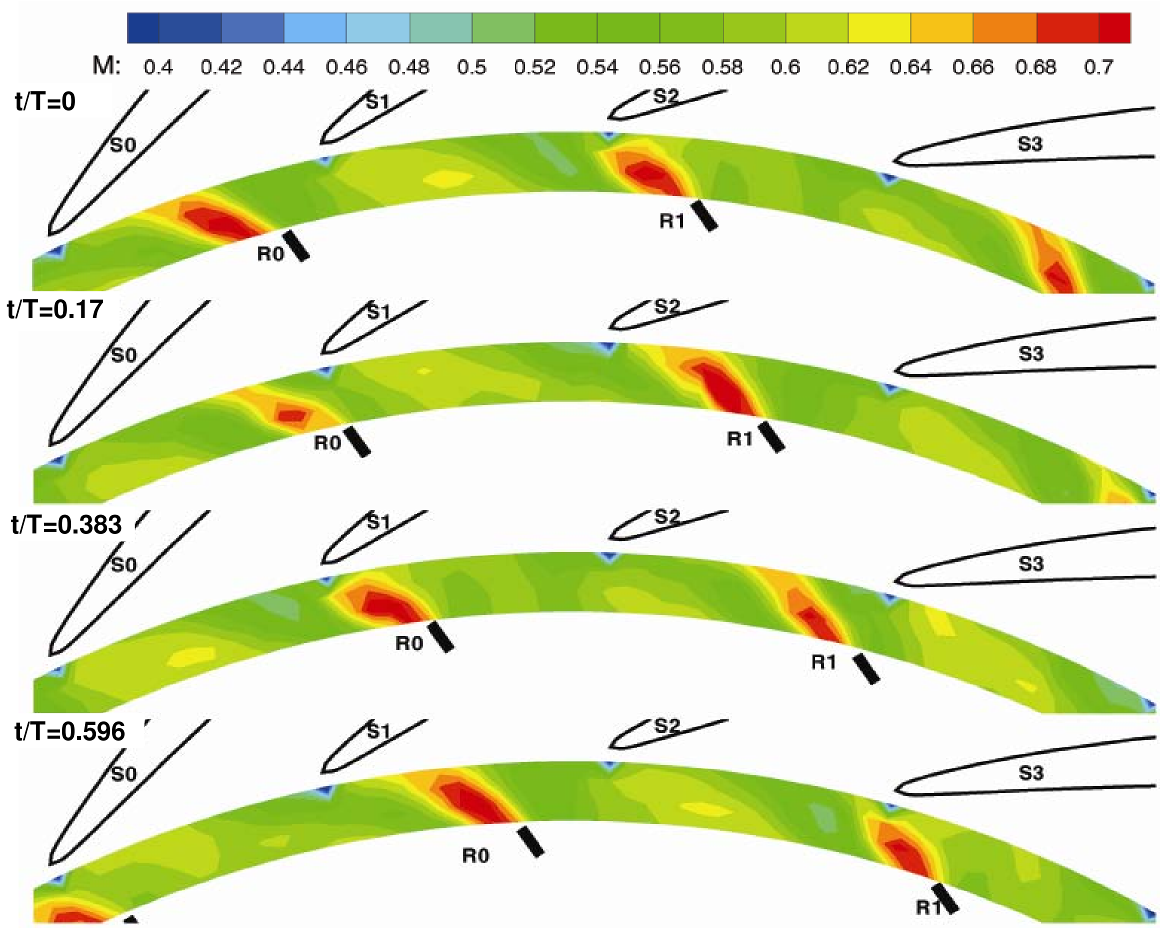

Figure 11. MACH NUMBER SNAPSHOTS AT FOUR IMPELLER-DIFFUSER POSITIONS AT h/h_2=38%

Only at 80% span, in fact, the flow is aligned with the mean geometrical direction. Beside the effects on the diffuser performance (that is beyond the aim of the present paper), such high spanwise incidence variation induces a variation of the front loading of the diffuser vanes and the stagnation point moves from the suction side at the hub to the pressure side at the tip. This results in a strong change in the propagation of the vane upstream potential field.

Figure 10 reports the radial distribution of TKE at the beginning of the period. In this map two impeller channels and three diffuser channels are fully visible. Due to the unequal blade numbers (16/25, roughly equal to 2/3), a phase lag of

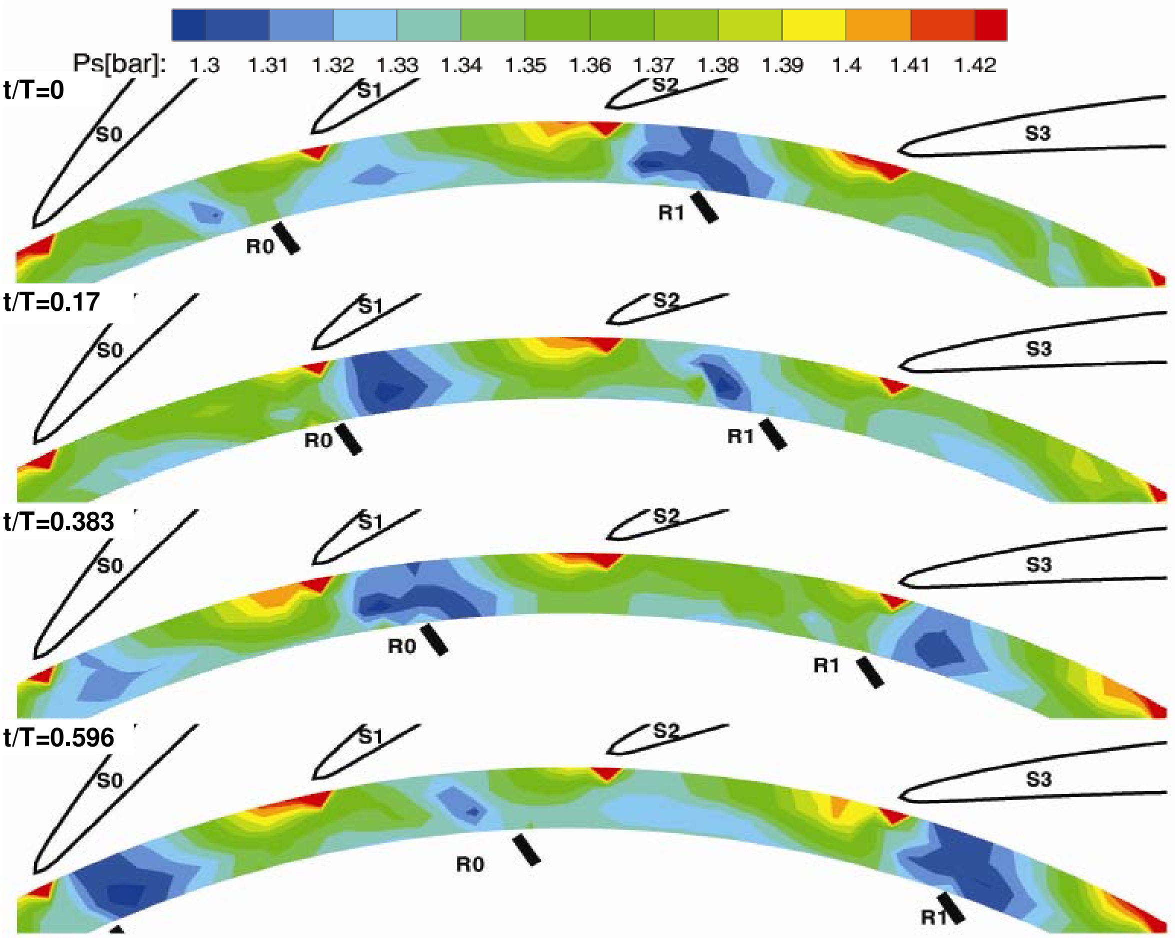

Figure 12. STATIC PRESSURE SNAPSHOTS AT FOUR IMPELLER-DIFFUSER POSITIONS AT h/h_2=38%

about the half of the period exists between adjacent channels. As a consequence at t/T = 0.0 the rotor wake shed by blade R0 enters in the middle of the diffuser channel between S0 and S1, while the one shed by the blade R1 directly impinges on the S2 leading edge. The wakes are shed along the mean direction of the relative velocity, and their radial evolution is weakly affected by the diffuser blades, unless they impinge directly on the leading edge of the airfoils. The total pressure field, also reported in Fig. 10, is also almost independent of the diffuser blades position, and its streamwise variation seems only linked to diffusion.

Although the wake turbulent content is almost unaffected by the diffuser vane potential field, the over-speed region on the impeller blade suction side is significantly modulated by the interaction. Figure 11 reports four interaction instants (or phases) and shows the periodic evolution of the Mach number. Due to the aforementioned phase-lag between adjacent channels, the relative R0-S1 position at t/T=0 is repeated between R0 and S2 at t/T=0.64. The high Mach number jet weakens when the rotor blade is faced to the diffuser vane, as it occurs for blades R0 and S1 at t/T=0.17 or for blade R1 and S3 at t/T=0.383. Conversely, when the rotor blade trailing edge is faced to the stator passage the Mach number increases. This blockage phenomenon occurs periodically as the rotor blades sweep the diffuser passage, making the rotor passage flow rate and the work exchange to be highly unsteady.

The origin of the pulsation is the potential field generated by the diffuser vanes, highlighted by the unsteady static pressure field reported in Fig. 12. The high pressure level on the vane leading edge, related to the stagnation streamline, propagates towards the impeller roughly along the mean absolute velocity direction. Depending on the interaction phase, the vane upstream pressure field interacts with the one induced by the impeller blades, resulting in a complex, fully unsteady pressure pattern in between the blade rows. For example at t/T=0.17 for blades R0–S1 the pressure field interaction leads to a high pressure level on the impeller blade suction side, while at t/T=0.383 the same blade has a low pressure on both blade sides, since the blade is completely facing the stator passage. At t/T=0.596 the cycle on blade R0 completes and a high pressure is found on the blade pressure side; the periodic pressure fluctuation is about 50 mbar (± 2% of the mean value). It is interesting to note that, when the pressure level on the impeller blade suction side is high (t/T=0.17, R0), the Mach number on

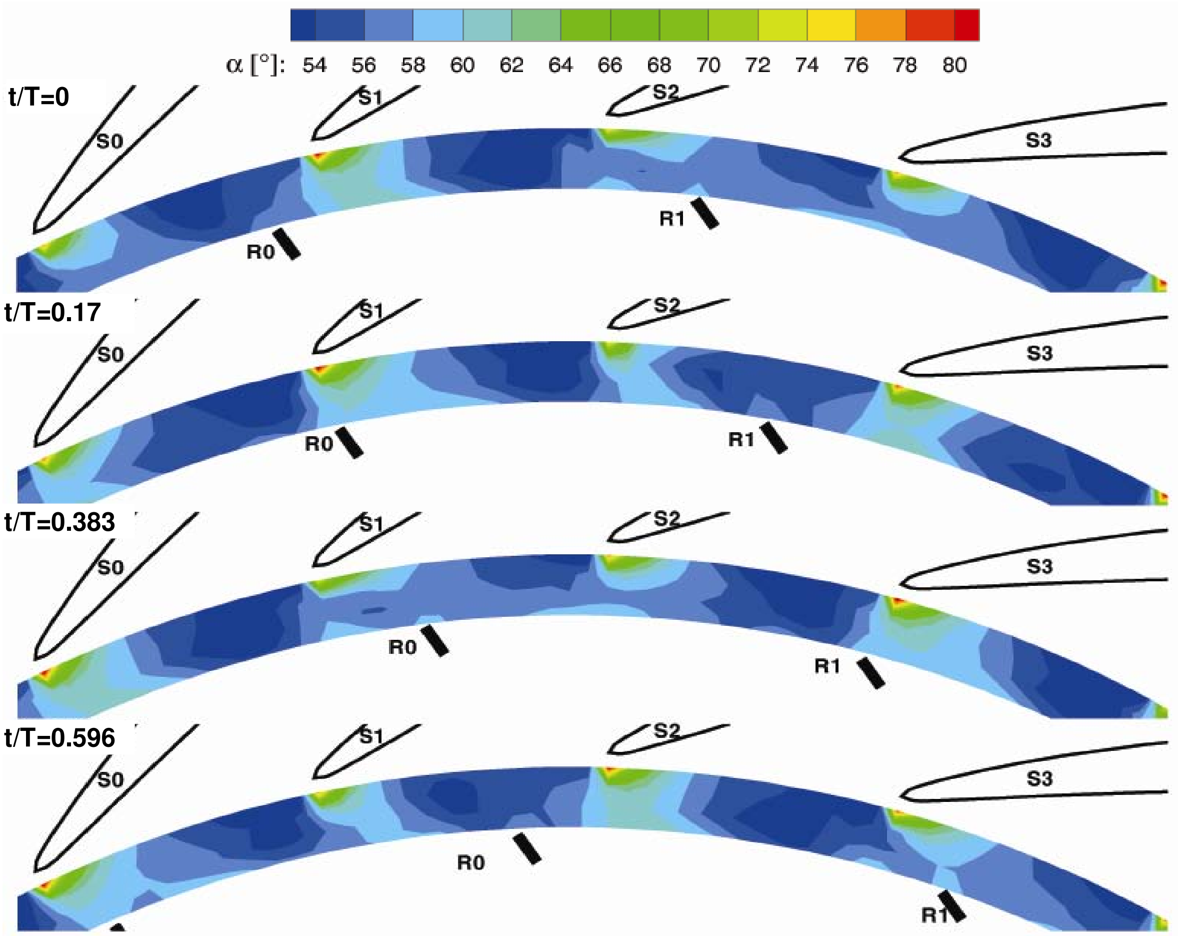

Figure 13. FLOW ANGLE SNAPSHOTS AT FOUR IMPELLER-DIFFUSER POSITIONS AT h/h_2=38%

the suction side jet is low; the opposite is found when the pressure level is low. As a final remark results indicate that the pressure on the rear sides of the rotor blade changes significantly, making even questionable the conventional pressure/suction side definition when applied to impeller blades operating upstream of a vaned diffuser; by an average point of view, a pressure/suction relationship is evidently required for the work exchange.

Coupled to the pressure field, the flow angle undergoes a significant fluctuation too, as shown in Fig. 13. As a general consideration, the flow angle changes significantly around the vane leading edge due to the flow turning imposed by the vane. A highly tangential flow is found on the vane suction side while a more radial flow occurs approaching the pressure side. Figures 12 and 13 clearly show that the direction of maximum flow deflection, roughly radial, does not coincide with that of the stagnation streamline. This produces a phase-shift between the pressure and velocity perturbations acting on the rear part of upstream impeller blades. From the quantitative point of view the vane upstream potential field induces strong flow angle oscillations (up to 10 deg.) close to the impeller (at traverse R1, see for example blade R0 suction side at t/T=0 and at t/T=0.383), making the flow field in the rotating frame highly unsteady. The phase shift between the direction disturbances and the pressure one makes the velocity field very complex and strongly periodic for each rotor passage.

As a concluding remark, by comparing the time-mean and the instantaneous data it is clear how the averaging produces a dramatic loss of information on the actual flow field. In particular, the static pressure field of the rear part of the impeller blade results from the complex mutual diffuser/impeller interaction.

Considering now the tip region, where the maximum dissipation is found, a different potential field propagation is found, as reported in Fig. 14 only for t/T=0. This is caused by the more tangential flow. In particular, as the stagnation line is more tangential, the pressure field propagates towards the vane suction side more than that which happens at h/h_2=38%; on the contrary, the flow deflection imposed by the presence of the vane propagates in the same direction recognized for h/h_2=38%. The final result is an increase in the phase shift between the two effects that makes the interaction process to be different along the blade height. The prediction of the overall effects on the diffuser performance, as well as the detailed investigation of the

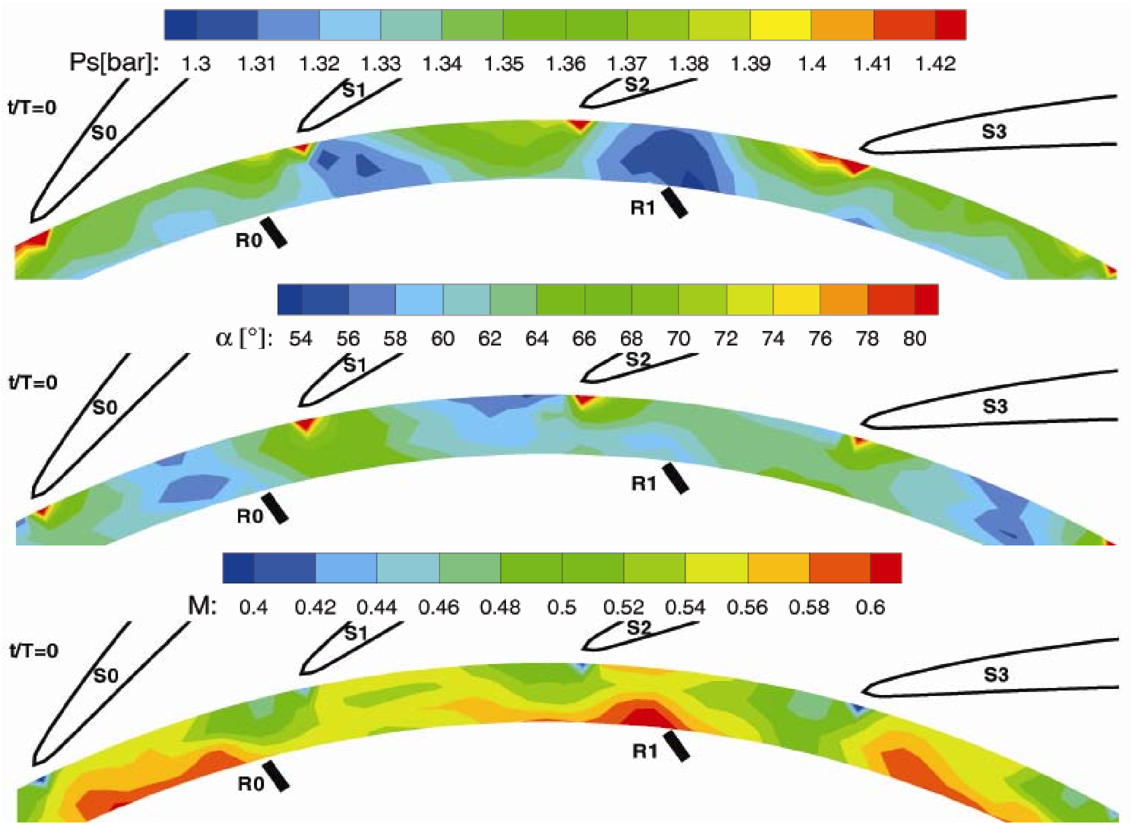

Figure 14. STATIC PRESSURE, FLOW ANGLE AND MACH NUMBER SNAPSHOTS FOR t/T=0 AT h/h_2=72.5%

interaction phenomena, requires the application of unsteady CFD.

In order to quantify the magnitude of the fluctuation on one impeller passage, the averages on a single passage at traverse R1 were also computed for different impeller/diffuser phases. If static pressure is of concern, the average value over a single impeller passage fluctuates of 6 mbar, which is 0.5 % of the mean value. The corresponding radial loading fluctuation on the bearings is therefore negligible. On the same passage, the mass flow rate has a fluctuation of 2%, while the work unsteadiness is of about 1%. The exchanged power, combination of work times flow rate, fluctuates of about 2%, corresponding also to the fluctuation of the pressure field on the impeller blades surface, being the rotational speed constant.

CONCLUSIONS

This paper reviewed an analysis of the impeller - vaned diffuser interaction by means of unsteady flow measurements in the vaneless region supported by CFD calculation inside the impeller. At first the analysis has been focused on the impeller time-mean flow in the rotating frame. In this context, CFD has been proven to provide reliable qualitative and quantitative results at traverses close to the impeller trailing edge.

The turbulent kinetic energy measured at the impeller outlet, analysed with the aid of the computed flow field inside the channel, shows that the main secondary and dissipative structure is the tip leakage vortex, the impeller under consideration being unshrouded. The distortion imposed by the smoke-shelf geometry amplifies the dissipative structures in the tip region and induces strong spanwise (axial) gradients at the exit of the impeller. Measurements have shown that, for the present design, the conventional assumption of jet/wake flow field is rather limited when a detailed analysis of the periodic flow is performed.

The second part of the paper has considered the impeller-vaned diffuser interaction. Measurements have shown that the flow field at the impeller exit is modulated by the diffuser blade in a different way depending on the interaction position and on the quantities of interest. For example total pressure is weakly affected by the diffuser which, on the contrary, modifies the flow velocity and direction and the static pressure, as well. The potential pressure field is seen to act directly on the Mach number which undergoes a significant reduction in magnitude when the high speed flow impinges on the diffuser vane leading edge. At the same time the deflection imposed by the presence of the vane propagates in a different direction with respect to the pressure field generating a phase shift between the interaction effects on the rotor pitch.

Moreover, the intensity of the diffuser potential field is a function of the magnitude of the flow field discharged by the impeller, namely of the impeller position, making the prediction of its effect a very complex task; the complexity of the flow configuration is further enhanced by the spanwise non-uniformity.

Furthermore, when an interaction process with a vaned diffuser takes place, the pressure field at the impeller exit is strongly modulated, even at the design point, showing that the definition of pressure side / suction side of the impeller blade is somehow questionable, when applied to the rear part of the blade. Finally, since the main source of interaction is the vane potential field, it is expected that the radial gap between the impeller and the diffuser blades determines the level of interaction. A future study will focus on the effects of this interaction on the diffuser performance.

NOMENCLATURE

a	sound speed
d, D	radial coordinate, diameter
EXP	experimental
h	blade / vane span
Mach	Mach number
Q	volumetric flow rate
P	pressure
RPM	revolution per minute
SW	streamwise position
t , T	time, impeller blade passing period
TKE	turbulent kinetic energy
U	peripheral speed
α	absolute flow angle in the blade to blade plane; taken from the radial direction
δ	deviation angle: flow angle – blade angle, both of them taken from the radial direction
ω	vorticity

subscript:

0	impeller inlet
2	impeller outlet
3	vaned diffuser inlet
Rel	relative
s	streamwise, static
T	total

ACKNOWLEDGMENTS

Authors wish to thank Mr. P. Grigatti and Mr. C. De Ponti for their valuable contribution in the instrumentation and preparation of the test rig.

REFERENCES

[1] Cumpsty, N. A., 1989. “Compressor Aerodynamics”, *Longman Scientific&Technical, England.*

[2] Japikse, D., 1996. “Centrifugal Compressor Design and Performance”, *Concepts ETI, Inc.*

[3] Krain, H., 2005. “Review of Centrifugal Compressor’s Application and Development”, *Journal of Turbomachinery*, Vol. 127, pp. 25- 34.

[4] Tapinassi, L., Fiaschi, D. Manfrida, G., 2006. “Improving the Accuracy of Tests for Centrifugal Compressor Stage Performance Prediction”, ASME ESDA International Conference on Engineering Systems Design and Analysis.

[5] Scotti Del Greco, A., Biagi, F., Sassanelli, G., Michelassi, V., 2007. “A New Slip Factor Correlation for Centrifugal Impellers in a Wide Range of Flow Coefficients and Peripheral Mach Numbers”, ASME Paper GT2007-27199.

[6] Ziegler, K.U., Gallus, H., Niehuis, R., 2003. “A Study on the Impeller-Diffuser Interaction – part I: Influence on the Performance” *Journal of Turbomachinery*, Vol. 125, Issue 1, pp 173-182.

[7] Ziegler, K.U., Gallus, H., Niehuis, R., 2003. “A study on the Impeller-Diffuser Interaction – part II: Detailed Flow Analysis” *Journal of Turbomachinery*, Vol. 125, Issue 1, pp 183-192.

[8] Schleer, M., Hong, S.S., Zangeneh, M., Roduner, C., Ribi, B., Ploger, F., Abhari, R.S., 2004. “Investigation of an Inversely Designed Centrifugal Compressor Stage-Part II: Experimental Investigation” *Journal of Turbomachinery*, Vol. 126, pp 82-90.

[9] Krain, H., 1981. “A Study on Centrifugal Impeller and Diffuser Flow”, *Asme J. Eng. Power* 103, pp 688-697.

[10] Hah, C., Krain, H., 1989. “Secondary Flows and Vortex Motion in a High-Efficiency Backswept Impeller at Design and Off-Design Conditions” Asme paper 89-GT-181, Gas Turbine and Aeroengine Congress Exposition, June 4-8-1989, Toronto- Canada.

[11] Shum, Y.K.P., Tan, C. S., Cumpsty, N. A., 2000. “Impeller – Diffuser Interaction in a Centrifugal Compressor” *Journal of Turbomachinery*, Vol 122. pp 777-786.

[12] Filipenco, V. G., Deniz, S., Johnston, J. M., Greitzer, E. M., Cumpsty, N. A., 2000. “Effects of the Inlet Flow Field Conditions on the Performance of centrifugal Compressor Diffuser: Part 1 – Discrete Passage Diffuser” *Journal of Turbomachinery*, Vol. 125, pp 1-10.

[13] Deniz, S., Greitzer, E. M., Cumpsty, N. A., 2000. “Effects of the Inlet Flow Field Conditions on the Performance of centrifugal Compressor Diffuser: Part 2 – straight Channel Diffuser” *Journal of Turbomachinery*, Vol. 125, pp 11-21.

[14] Persico, G., Gaetani, P., and Guardone, A., 2005. "Design and Analysis of New Concept Fast-Response Pressure Probes", Measurement Science and Technology, Vol. 16, N° 9, pp. 1741-1750.

[15] Persico, G., Gaetani, P., Paradiso, B., 2008. "Estimation of Turbulence by Single-Sensor Pressure Probes", Proceedings of the XIX Biannual Symposium on Measuring Techniques in Turbomachinery Transonic and Supersonic Flow in Cascades and Turbomachines, April 7-8, Rhode-St-Genese, Belgium.

[16] Gaetani, P., Persico, G., Dossena, V., Osnaghi, C., 2007. “Investigation of the Flow Field in a HP Turbine Stage for Two Stator-Rotor Axial Gaps: Part II –Unsteady Flow Field.” Journal of Turbomachinery, Vol. 129, pp. 580-590.

[17] Toni, L., Ballarini, V., Cioncolini, S., Gaetani, P., Persico, G., 2010. “Unsteady Flow Field Measurements in an Industrial Centrifugal Compressor” 39th Turbomachinery Symposium - October 4-7, Houston, Texas